Applied Catalysis B: Environmental 164 (2015) 217–224

Contents lists available at ScienceDirect

Applied Catalysis B: Environmental

journal homepage: www.elsevier.com/locate/apcatb

Full Length Article

Plasmon-induced photoelectrocatalytic activity of Au nanoparticles enhanced TiO_2 nanotube arrays electrodes for environmental remediation

Ling Wu [1], Fang Li [1], Yuanyuan Xu, Jane W. Zhang, Dieqing Zhang, Guisheng Li *, Hexing Li

Key Laboratory of Resource Chemistry of Ministry of Education, Shanghai Key Laboratory of Rare Earth Functional Materials, College of Life and Environmental Science, Shanghai Normal University, Shanghai, 200234, China (PRC)

ARTICLE INFO

Article history:
Received 5 August 2014
Received in revised form 9 September 2014
Accepted 14 September 2014
Available online 23 September 2014

Keywords:
Au
TiO_2
Photoelectrocatalytic
Plasmon-induced
Environmental remediation

ABSTRACT

A pulse electrodeposition (PED) technique was adopted to construct highly dispersed Au nanoparticles (Au-NPs) on TiO_2 nanotube arrays (TiO_2-NTs) electrodes prepared by electrochemical anodic oxidation. Both the particle size and loading amount were facilely controlled via adjusting electrochemical parameters. The morphology, crystallinity, elemental composition and light absorption capability of as-obtained Au/TiO_2-NTs were distinguished based on various characterizations. Compared with pure TiO_2-NTs, Au/TiO_2-NTs electrodes exhibited much higher photocurrent density and greatly enhanced photoelectrocatalytic (PEC) activity towards the degradation of methyl orange (MO) under visible-light irradiation ($\lambda > 420$ nm). The synergy effect between nanotubular structures of TiO_2 and uniformly dispersed Au nanoparticles, as well as the small bias potential and strong interaction between Au and TiO_2, facilitated the Au plasmon-induced charge separation and transfer, which lead to highly efficient and stable visible-light PEC activity.

1. Introduction

A well-aligned TiO_2-NTs fabricated by electrochemical anodization has been demonstrated to be a promising photoanode for applications in water purification [1–3], hydrogen generation [4,5], antimicrobial [6,7], and photovoltaic cell energy generation [8,9]. The benefits of TiO_2-NTs include its large specific surface area, excellent mechanical adhesion, excellent electron percolation pathway, and facile synthesis process. Nevertheless, TiO_2-NTs is far from being a perfect photocatalyst, largely due to the limitation of its large band gap, which results in poor efficiency upon visible light irradiation. One of the effective approaches to overcome such an impediment is to load noble metal, particularly Au NPs, onto the surface of TiO_2-NTs. Gold is stable enough to resist corrosion under photocatalytic conditions, and it exhibits a characteristic surface plasmon band in the visible-light region, owing to the collective excitation of electrons [10,11].

It is well known that the catalytic properties of gold nanoparticles on supporting materials depend heavily upon the metal particle size, dispersion, and composition, etc. [12]. A high dispersity of nanoparticles on TiO_2-NTs was favorable for visible-light response and charge separation, which resulted in better catalytic performance. Therefore, it is highly important to ensure uniform dispersion and tunable particle size on TiO_2-NTs in order to promote its catalytic activities. To date, several studies have focused on the preparation of Au-NPs supported on TiO_2, including sputtering [13], photo-reduction [14,15], deposition–precipitation [16] etc. Based on these methods, the Au-NPs will generally grow large and aggregate on the surface easily. In order to further enhance catalytic activity, there is a need to choose a more effective technique to obtain high-quality Au/TiO_2-NTs with sufficiently small Au-NPs homogeneously dispersed on geometrically ordered TiO_2-NTs.

Recently, Lai et al. [17] reported a pulse current deposition route for growing noble metal (Ag) nanoparticles. Such route was proven to be effective for both refining the size of the crystal particles and obtaining a homogeneous surface appearance. In pulse electrodeposition (PED), the current is alternated swiftly between two different values. Each pulse consists of an on-time (t_{on}) period, during which potential and/current is applied, and an off-time (t_{off}) period, during which zero current is applied. Such a route contains two advantages [18]: (a) PED significantly raises the limiting current density by replenishing metal ions in the diffusion layer only during t_{off}; (b) The size and dispersion of metal particles on the

* Corresponding author. Tel.: +86 21 64321673; fax: +86 21 64322272.
E-mail address: Liguisheng@shnu.edu.cn (G. Li).
[1] Equal contribution.

http://dx.doi.org/10.1016/j.apcatb.2014.09.029
0926-3373/

surface of carriers can be easily achieved by changing the electrochemical parameters such as peak potential, on-time, off-time and pulse cycles. Thus, it is reasonable that PED could provide a feasible way for fabricating ideal Au/TiO_2-NTs composites. In this work, metallic Au-NPs loaded TiO_2 nanotube-arrays electrodes were prepared by PED method. Both of the photo-electrochemical properties and the photoelectrocatalytic activity towards the degradation of MO were examined using the as-formed Au/TiO_2-NTs composites as photoanodes. Such Au/TiO_2-NTs composites exhibited excellent plasmon-induced photoelectrocatalytic activity for degrading MO molecules with high stability under visible-light irradiation ($\lambda > 420$ nm).

2. Experimental

2.1. Preparation of Au loaded TiO_2 Nanotube arrays electrodes

Pure TiO_2-NTs electrodes were fabricated through potentiostatic anodization in a two-electrode electrochemical cell, using a titanium sheet (0.3 mm thick, 99.5% purity, Shanghai Right Titanium Industry Co., Ltd., China) as a working electrode and a Pt plate as a counter electrode. Before using, the titanium sheets were rinsed in an ultrasonic bath of acetone, ethanol and distilled water, in that order, for 10 min each round. Then the cleaned titanium sheets were soaked in a mixture of 0.2 M NH_4F and 0.1 mol L^{-1} H_3PO_4 for 7 h at 20 V. The as-anodized samples were crystallized through ambient annealing (500 °C) at a heating rate of 2 °C/min.

The Au/TiO_2-NTs electrodes were prepared through PED technique using an electrochemistry station (CHI 660D) to control the deposition potential. A three-electrode setup was applied using the TiO_2-NTs as the working electrode, a Pt sheet as the counter electrode, and a saturated calomel electrode (SCE) as the reference electrode (Fig. S1). The TiO_2-NTs working electrodes were ultrasonically cleaned in 1 mmol L^{-1} $HAuCl_4$ aqueous solution for 6 min in the dark to remove surface contaminants and drive the air out of the nanotubes. Au-NPs were then deposited onto the crystallized TiO_2-NTs using a potential pulsing approach, which involved switching between a cathodic pulse (−3 V, 50 ms) and a short-circuit pulse (0 V, 100 ms) at room temperature. Deposition time was fixed at various pulse cycles, and the samples obtained correspondingly were denoted as *x*-Au/TiO_2-NTs (*x* = 50, 100, 200, 500 and 800).

2.2. Characterization

Wide-angle X-ray diffraction measurements were carried out in a parallel mode ($\omega = 0.5°$, 2θ varied from 20° to 80°) using a Rigaku Dmax-3C Advance X-ray diffractometer (Cu Kα radiation, $\lambda = 1.5406$ Å). The morphologies of the products were observed and analyzed through a field emission scanning electron microscopy (FESEM, S-4800). The surface electronic states were analyzed through X-ray photoelectron spectroscopy (XPS, Perkin-Elmer PHI 5000). All the binding energy values were calibrated using C1s = 284.6 eV as a reference. The diffuse reflectance spectra of the samples over a range of 200-800 nm were recorded by a Varian Cary 500 UV–Vis-NIR system equipped with a Labsphere diffuse reflectance accessory by using $BaSO_4$ as a reference. ·OH-trapping photoluminescence spectra were recorded on a photoluminescence spectrum (PLS, Varian Cary-Eclipse 500) ($\lambda_{ex} = 312$ nm).

2.3. Photoelectrochemical and photoelectrocatalytic Measurements

Photoelectrochemical measurements were carried out in a conventional three-electrode, homemade single-compartment quartz cell on an electrochemical station (CHI 660D). The Au/TiO_2-NTs electrode with an active area of ca. 4 cm^2 was served as a photoanode, the Pt sheet served as cathode, and the SCE served as the reference electrode. A 0.1 mol L^{-1} Na_2SO_4 aqueous solution (50 mL) was used as a supporting electrolyte. A 300 W Xe lamp with an ultraviolet filter ($\lambda > 420$ nm) was used as the visible-light source and positioned 14 cm away from the photoelectrochemical cell. A bias potential of 0.6 V vs. SCE was applied on the photoanode for the photocurrent test under on-off light conditions.

The liquid-phase photoelectrocatalytic activity of Au/TiO_2-NTs was evaluated by the level of degradation of methyl orange (MO) with an initial concentration of 5 mg L^{-1}. The setup and other reaction conditions were the same as those of photoelectrochemical measurements. Upon being vigorously stirred for 1 h in order to reach the adsorption-desorption equilibrium of MO on the catalyst, the photoelectrochemical reaction was initiated by irradiating the system with visible light. At given irradiation time intervals, ca. 3 mL of reaction solution was sampled, and the residual MO concentration was analyzed using a UV spectrophotometer (UV 7504/PC) at the solution's characteristic wavelength ($\lambda_{MO} = 467$ nm). For comparison, the photoelectrocatalytic experiments for a pure TiO_2-NTs electrode were also performed under identical conditions. No more than 2% of pollutants were degraded in a direct photolytic process without using a working electrode. And the reproducibility was checked by repeating the results at least three times, and was found to be within acceptable limits.

3. Results and discussion

3.1. Composites characterization

As shown in Fig. 1, An Au/TiO_2-NTs electrode was fabricated *via* an anodic oxidation process and pulse-electrodeposition route [19–21]. During the Au pulse-electrodeposition process, a multi-current-steps technique was utilized for loading Au-NPs on TiO_2-NTs by controlling the deposition potential to induce PED and choosing 1.0 mmol L^{-1} $HAuCl_4$ aqueous solution as the electrolyte (the PED graph showed in Fig. S2). In the reaction system, there is a $[AuCl_4]^{-1}$ concentration gradient in the solution. The concentration of $[AuCl_4]^-$ in the solution close to the TiO_2-NT surface is lower than that in the solution far from the electrode. The electro-ionization equation of $[AuCl_4]^-$ in the plating solution can be expressed as Eq. (1), and the electrodeposition of the Au-NPs on the surface of TiO_2-NTs can be depicted as Eq. (2) [22].

$$[AuCl_4]^- \rightleftarrows Au^{3+} + 4Cl^- \quad (1)$$

$$Au^{3+} + 3e^- \rightarrow Au \quad (2)$$

The ionization balance will shift to the right side as the consumption of Au^{3+} in the reduction reaction, which could induce the diffusion of $[AuCl_4]^-$ from bulk solution onto the electrode surface. The concentration of $[AuCl_4]^-$ in the electrode interface is supplemented during the off period in the PED process, which reduces the concentration polarization efficiently, and consequently triggers the reduction reaction occurring under the high current density to promote the formation speed of seed crystals for the purpose of grain refinement. In order to determine the deposition potential of Au-NPs on TiO_2-NTs surface in 1 mmol L^{-1} $HAuCl_4$ solution, a cyclic voltammogram curve with the range of scanned potentials from −1.5 V to 1.5 V was obtained using pure TiO_2-NTs as the work electrode, Pt foil as the counter electrode, and SCE as the reference electrode, as shown in Fig. S3a. A wide reduction peak around −0.6 V appears in the curve, which is recognized as the reduction of Au^{3+} on TiO_2-NTs. However, upon choosing a −1.0 V deposition potential, serious aggregation of Au-NPs on the top of TiO_2-NTs was observed (Fig. S3b). Further increasing the PED potential to −3.0 V produced well- dispersed Au-NPs with narrow size distribution, as

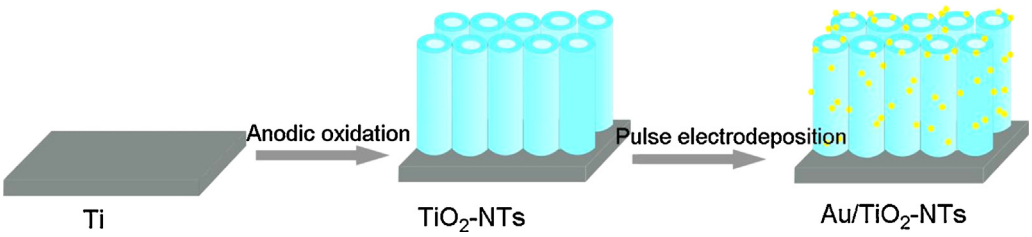

Fig. 1. Schematic process for synthesizing Au/TiO_2-NTs electrode.

shown in Fig. S4c. This phenomenon could be explained by the fact that high over-potential is deemed to increase nucleation rate by increasing the free energy for formation of new nuclei [23]. These results indicated that the potential applied in the deposition procedure could significantly influence the surface morphology of the Au/TiO_2-NTs. Thus, the PED potential is fixed at −3.0 V vs. SCE in the present work.

The morphologies of TiO_2-NTs electrodes were characterized by field emission scanning electron microscopy (FESEM). Fig. 2a and b displays the typical top-view and side-view FESEM images of the pure TiO_2-NTs. One can see that the pure TiO_2-NTs possesses highly ordered structure and vertical orientation with an average outer pore diameter of ca. 100 nm, wall thickness of ca. 10 nm, and tube length of ca.1.0 μm. Fig. 2c and d shows the FESEM images of 100-Au/TiO_2-NTs, which reveal that obtained Au-NPs were highly dispersed on both outside and inside of the TiO_2-NTs, as we would expect. Notably, both the size and the loaded amount of Au-NPs, which are extremely crucial to PEC activities, can be adjusted by varying the electrolyte concentration, on-off time, deposition potential, and deposition time (shown in Fig. S5). Regarding various deposition times, the size of the as-loaded Au-NPs could be increased from 8 to 40 nm by adjusting the pulse cycles from 50 to 800. These results confirmed that the further nucleation and growth of Au-NPs are likely to reduce the surface energy of the nanoparticles [21]. In order to identify the crystal phase of TiO_2-NTs and Au/TiO_2-NTs, the X-ray diffraction (XRD) result was considered with the results shown in Fig. 3. All samples clearly show the TiO_2 anatase phase (JCPDS No: 21-1272) and the Ti metal phase (JCPDS No: 44-1294). Upon increasing the deposition time, only one weak peak at 44.5° indexed to the Au (1 1 1) plane (JCPDF 04-0784) appears. Other diffraction peaks could not be observed, perhaps owing to the ultrafine size, high dispersity, and low concentration of Au-NPs. Such XRD results as presented are evidence of successful Au deposition with high dispersity and ultrafine crystal size using the PED approach.

Furthermore, X-ray photoelectron spectroscopy (XPS) was employed to analyze the elemental compositions of the TiO_2-NTs and Au/TiO_2-NTs in order to investigate the chemical states of Au and acquire in-depth fundamental information on the interaction between the deposited Au-NPs and TiO_2-NTs. The general scan

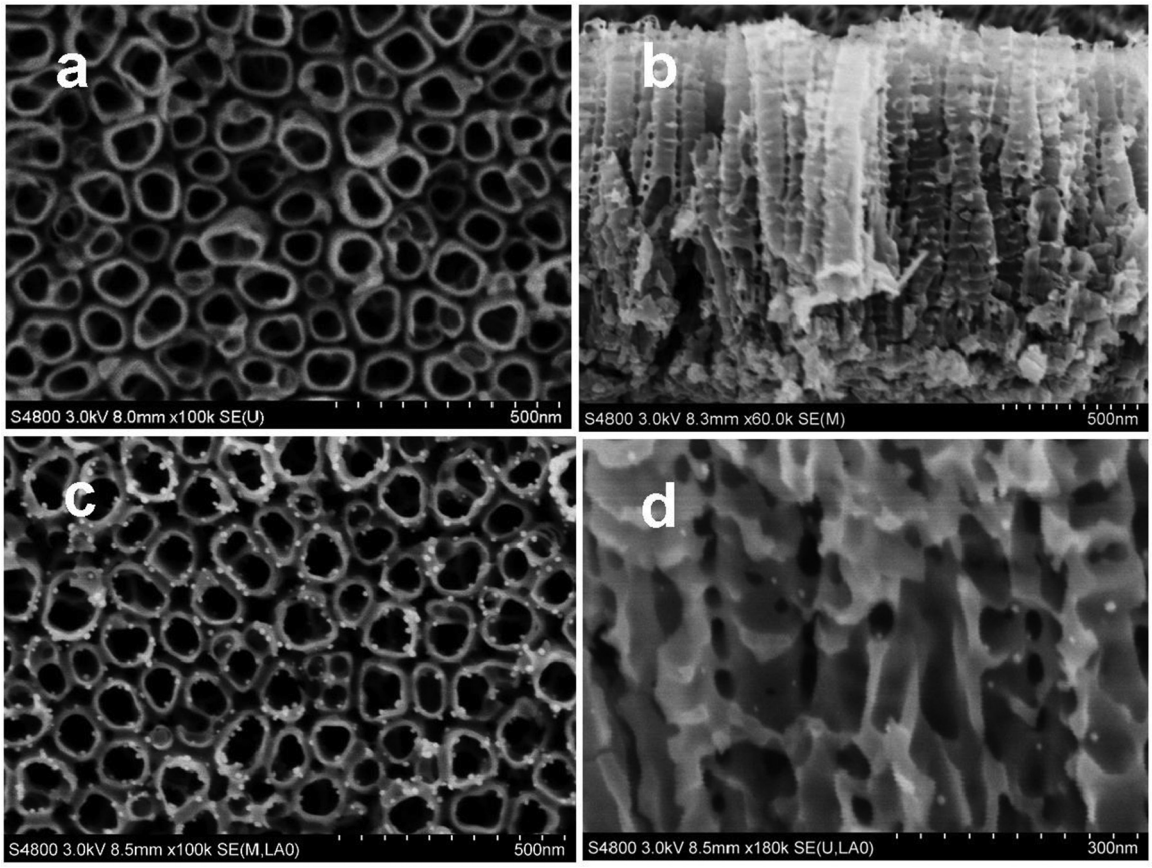

Fig. 2. FESEM images of pure TiO_2-NTs (a and b) and 100-Au/TiO_2-NTs (c and d).

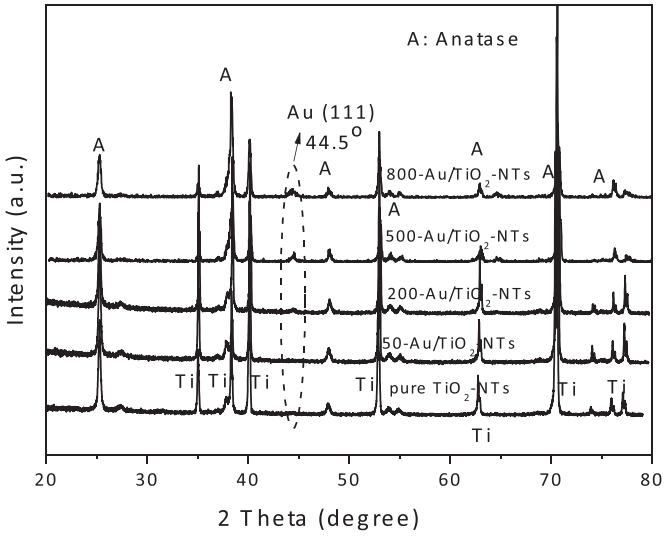

Fig. 3. XRD patterns of pure TiO_2-NTs and Au/TiO_2-NTs electrodes.

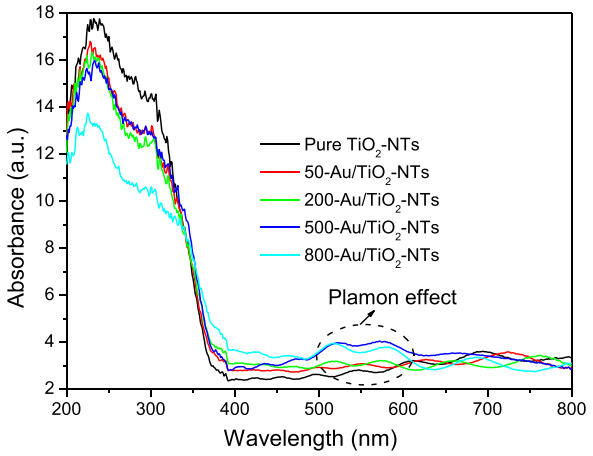

Fig. 5. UV–Vis diffuse reflectance spectra of pure TiO_2-NTs and Au/TiO_2-NTs electrodes.

spectrum of XPS over a large energy range at low resolution can be found in Fig. S6. It was detected that 800-Au/TiO_2-NTs electrode contains Ti, O, Au, and C. The high-resolution spectra of Au 4f and Ti 2p from the TiO_2-NTs electrode and 800-Au/TiO_2-NTs electrode were presented in Fig. 4a and b, respectively. The Au 4f spectra exhibited a $4f_{7/2}$ peak at 83.3 eV and an Au $4f_{5/2}$ peak at 86.9 eV, indicating that the as-formed Au NPs existed in mainly metallic Au state on the surface of TiO_2-NTs, which is well supported by the XRD analysis. It should be noted that a significant negative shift (ca. 0.7 eV) in the binding energy for Au $4f_{7/2}$ relative to 84.0 eV of the bulk Au [24] is apparent. The shift was due to the electron transfer from oxygen vacancies of the TiO_2 to Au, leading to a lower Au $4f_{7/2}$ core level binding energy in the Au/TiO_2-NTs [25]. Moreover, a positive shift of the Ti $2p_{3/2}$ after Au loading also revealed the feasibility of the electron transfer between the Au and TiO_2 [26].

Fig. 5 depicts the UV–vis diffuse reflectance spectra (DRS) of the pure TiO_2-NTs and Au/TiO_2-NTs electrodes. It has been observed that pure the TiO_2-NTs electrode exhibited a photo-response in the UV region with wavelengths below 380 nm, which can be attributed to intrinsic band gap of TiO_2. The weak absorption of pure TiO_2-NTs in visible-light region could be ascribed to the scattering of light caused by pores or cracks in the nanotube arrays [2,27]. After depositing Au-NPs, the Au/TiO_2-NTs composite electrodes exhibited visible-light absorption in the region ranging from 500 nm to 600 nm, due to localized surface plasmon resonance (LSPR) of Au-NPs on the pore-wall of the TiO_2-NTs. These results indicated that the photo-response of TiO_2-NTs could be easily extended to the visible-light region with the aid of Au-NPs as an inorganic sensitizer. Furthermore, it was noted that the absorption peaks in the visible-light region underwent red-shifts because LSPR of Au nanoparticle is size and distance dependent [28–30]. The formation of a LSPR can be explained as follows: the electric field of the incoming radiation induces the formation of a dipole in the Au nanoparticle. When the frequency of light photons matches the natural frequency of surface electrons' oscillations against the restoring force of positive nucleus, the LSPR is established [31]. The size of Au nanoparticle affects the natural frequency of surface electrons' oscillations. As known, bigger nanoparticle size could result in lower electron oscillation frequency, leading to light absorption in longer wavelengths. A localized electric field much stronger than that of a single nanoparticle could be generated in the gap between the nanoparticles when the inter-particle spacing is less than the particle diameter. The resonance wavelength would be red-shifted by the plasmon coupling effect [32–34]. It was also found that long deposition time favored the increase of the absorption intensity in visible-light region, and the decrease of UV absorption intensity. This phenomenon was not in accordance with the results reported by Li et al. [35] In the UV range, the Au/TiO_2 exhibited much stronger light absorbance than the pure TiO_2. This may be attributed to the higher concentration of Au in our system and the over-loaded

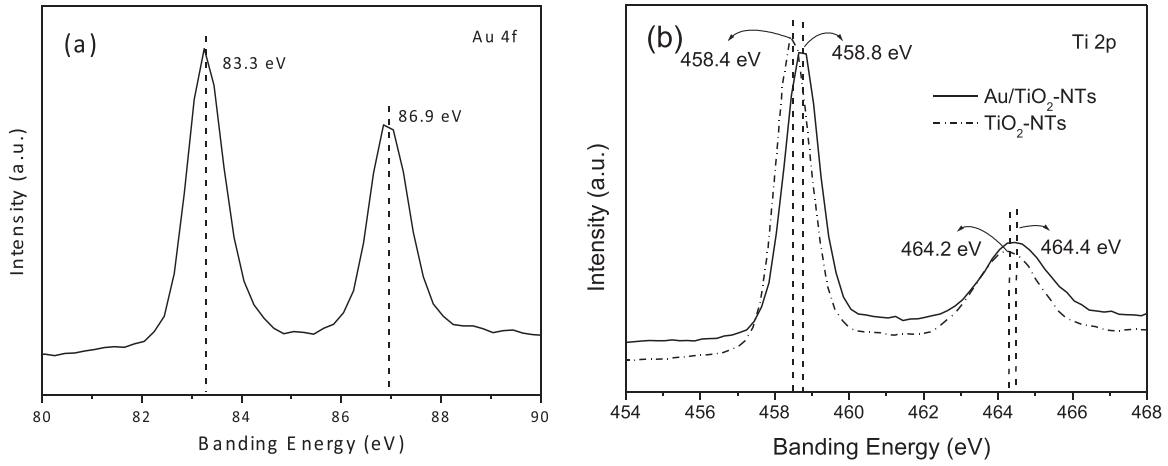

Fig. 4. XPS Spectra of TiO_2-NTs and 800-Au/TiO_2-NTs electrodes.

Au-NPs could cover the active surface of TiO_2-NTs, which would inhibit the UV light intrinsic absorption of TiO_2.

3.2. Photoelectrocatalytic activity

For evaluating the photoelectrochemical responses of as-prepared pure TiO_2-NTs and Au/TiO_2-NTs electrodes under visible-light irradiation, photocurrent densities were measured after using the light on-off process with a pulse of 10 s by potentiostatic technique. Upon being irradiated with visible-light ($\lambda > 420$ nm) at an applied potential of 0.6 V vs. SCE, all of the Au/TiO_2-NTs samples exhibited stronger photocurrents compared with pure TiO_2-NTs electrode, as shown in Fig. 6. For Au/TiO_2-NTs sample, the photocurrent value decreased to zero when visible light was turned off, and the photocurrent could immediately increase back to the original value when the light was turned on again. Such photocurrent responses were highly reproducible for numerous on-off cycles. It should be noted that the photocurrent underwent a period of decrease before it became steady. Such a period may be attributed to how the electrons could flow back from the TiO_2 conduct band to the Au-NPs. Thus, a small voltage was utilized to inhibit the feedback electrons from the TiO_2 conduct band to the Au in the PEC process. If the photocurrent was measured without voltage between the working electrode and the counter electrode (PC process), the photocurrent recorded was much lower.

The photoelectrocatalytic (PEC), photocatalytic (PC), and electrochemical (EC) processes for degrading methyl orange (MO) in aqueous solution were performed on the 800-Au/TiO_2-NTs electrode under visible-light illumination. As shown in Fig. 7a, no obvious degradation of MO could be observed after using the EC process, which indicated that the bias potential applied on the working electrode could not produce oxidative radicals on the anode surface needed for oxidizing MO molecules. We also noticed that only a 3% removal rate of MO was obtained during the PC process. Such low PC-induced activity could be attributed to the low quantum efficiency of the photoanodes. As known, the photocatalytic degradation of MO on the surface of Au/TiO_2-NTs was

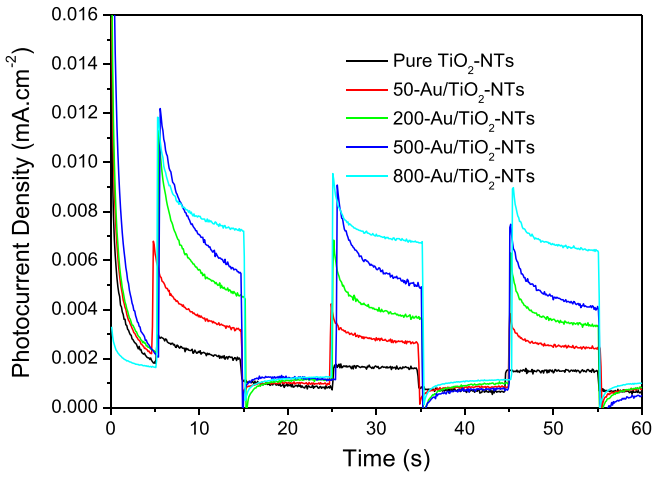

Fig. 6. Photocurrent response of pure TiO_2-NTs and Au/TiO_2-NTs electrodes in the on-off visible-light ($\lambda > 420$ nm) process.

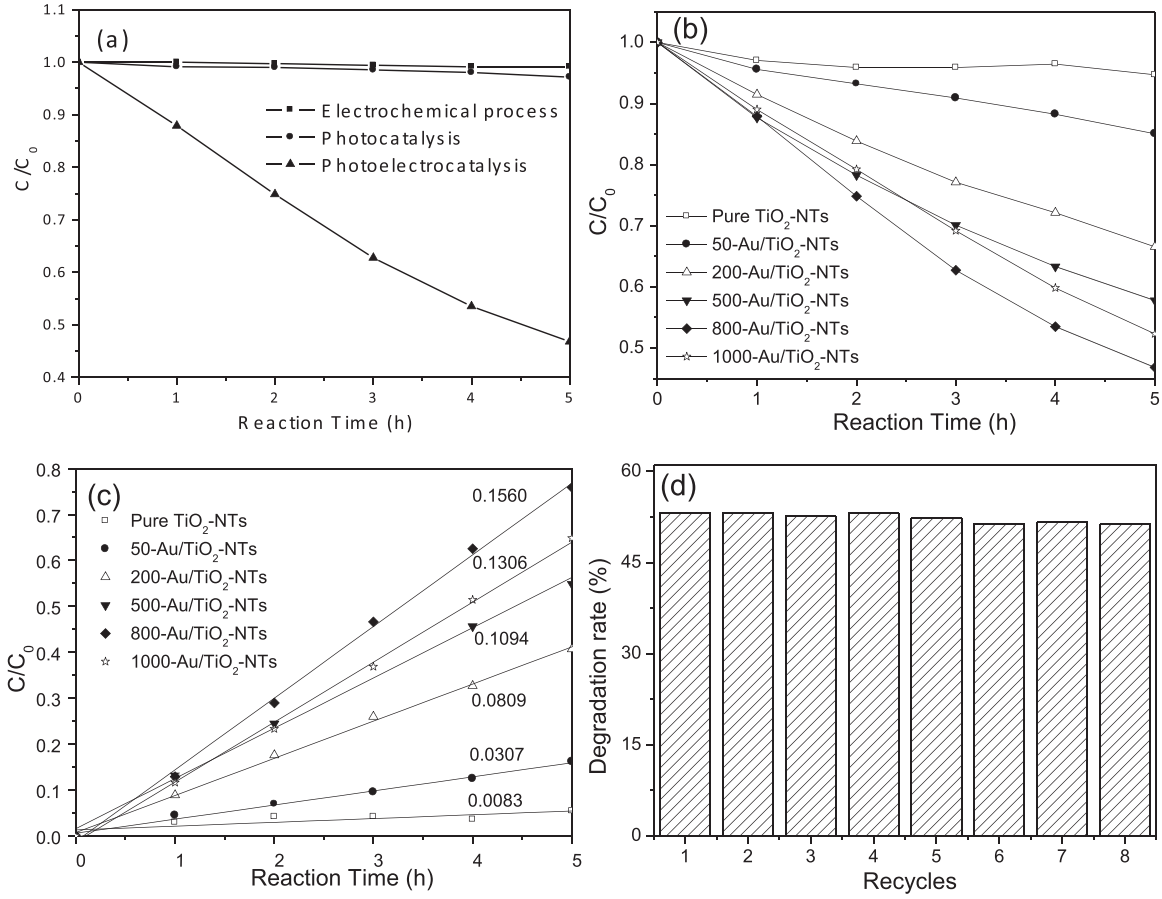

Fig. 7. (a) Degrading MO by photoelectrocatalysis, photocatalysis, and electrochemical process under visible-light irradiation *via* using Au/TiO_2-NTs as photoanodes ($\lambda > 420$ nm, 0.6 V vs. SCE bias potential); (b) The effect of pulse deposition time on PEC activities; (c) corresponding dependence of Ln(C_0/C) on irradiation time for degrading MO of various samples; (d) Recyclability of 800-Au/TiO_2-NTs electrodes for photoelectrocatalytic degrading MO under visible-light irradiation.

triggered by generated electrons on Au-NPs as a result of the plasmon effect. Such generated electrons could be further injected into the conduction band of TiO_2 with the formation of oxidative radicals. Nevertheless, such electrons trapped by the conduction band of TiO_2 would quickly transfer to the oxidized Au-NPs, resulting in low quantum efficiency for the photocatalytic degradation of MO under visible-light irradiation. Thus, it is highly required for exploring an effective route for the inhibition of the electron feedback from the conduction band of TiO_2 to Au. A much higher removal rate (54%) of MO was achieved upon using a 0.6 V bias between the working electrode (Au/TiO_2-NTs) and the counter electrode (Pt), to the case of the photoelectrocatalytic process. Such additional bias voltage between working electrode and counter electrode could induce the migration of photo-excited electrons to the counter electrode through the outer circuit, thereby preventing the recombination of electrons and the holes on the surface of Au and resulting in improved photocatalytic activity. These results demonstrated that the photoelectrocatalytic process was a feasible route for promoting the photo-induced charge separation of the Au/TiO_2-NTs, and, therefore, the most effective way to degrade MO molecules in aqueous solution. Fig. 7b also shows a comparison between the PEC performance regarding the degradation of MO using Au/TiO_2-NTs electrodes and pure TiO_2-NTs electrodes under visible-light irradiation ($\lambda > 420$ nm). As expected, the TiO_2-NTs electrode was devoid of any PEC activity under such conditions. On the other hand, all electrodes with loaded Au-NPs exhibited considerable photocatalytic performances. Such photoelectrocatalytic removal rate of MO could be recognized to follow mass-transfer-controlled first-order-kinetics approximately as a result of low concentration target pollutants as shown in Fig. 7c. Our former work has verified that well-dispersed CdS quantum dots enhanced TiO_2-NTs arrays' structures to allow the efficient usage of

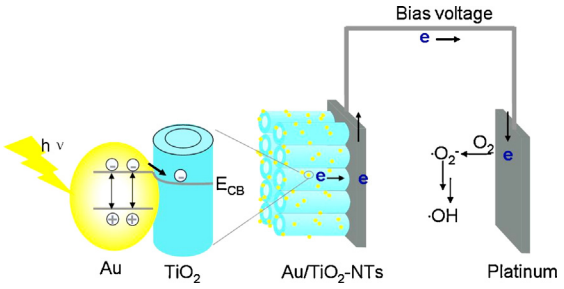

Fig. 8. Schematic diagram of the charge carrier transfer of photoelectrocatalysis for Au/TiO_2-NTs under visible-light irradiation.

visible-light and high charge separation efficiency [36]. Hence, the PEC activities here show that pulse electrodeposition is an effective method of obtaining nano-scaled architecture in favor of excellent PEC performance. It was also noted that the MO removal efficiency increased when the amount of Au-NPs below 800 cycles of electrodeposition was increased. This could be ascribed to the stronger absorption capability of visible-light region shown in the DRS test. The recyclability of the as-formed 800-Au/TiO_2-NTs electrodes was also investigated. As shown in Fig. 7d, no obvious decrease of activity was observed, suggesting the excellent stability of the photoelectrocatalytic electrodes. In all, the synergy between nanotubular structures of TiO_2 and uniformly dispersed Au grains on TiO_2, as well as a small bias potential, facilitated the plasmon-induced charge separation and transfer, thereby leading to high-efficiency visible-light PEC activity of Au/TiO_2-NTs.

A reasonable mechanism for the PEC process of MO degradation using Au/TiO_2-NTs as the photoanode was proposed (Fig. 8). Au-NPs could generate the photo-excited state of the Au based on

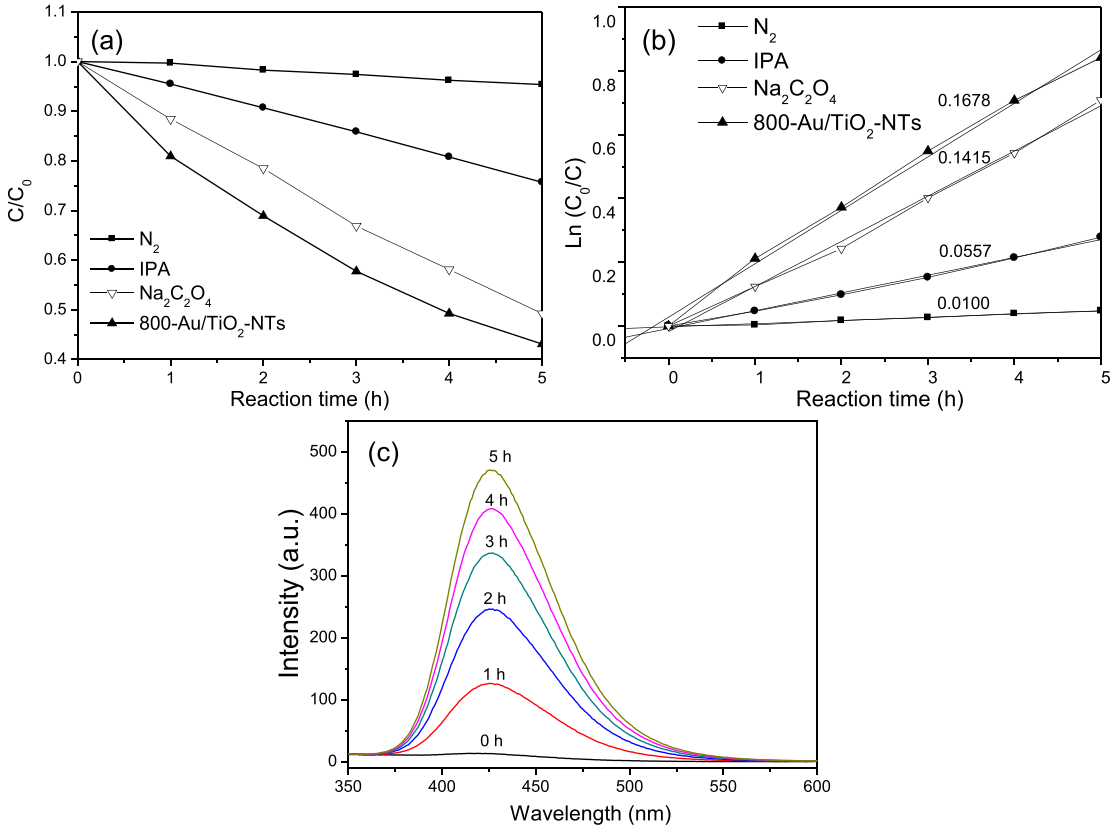

Fig. 9. (a) The effect of N_2, iso-propanol (IPA), and $Na_2C_2O_4$ on the photoelectrocatalytic performance of the 800-Au/TiO_2-NTs for degrading MO; (b) corresponding dependence of $Ln(C_0/C)$ on irradiation time for degrading MO; (c) ·OH-trapping photoluminescence spectra of 800-Au/TiO_2-NTs in 0.005 M terephthalic acid and 0.1 M NaOH solution at different irradiation time (λ_{ex} = 312 nm).

the located surface plasmon resonance under visible-light irradiation. A Schottky barrier was formed at Au/TiO_2-NTs interfaces due to the large work function of gold, so photo-excited electrons could easily transfer to the conduction band of TiO_2-NTs [37]. With the help of a small bias voltage between working electrode and counter electrode, the electrons would transfer along the TiO_2 nanotube arrays to the Ti substrate and eventually reach the counter electrode through outer circuit. Subsequently, the transferred electrons would further reduce the oxygen absorbed on the surface of counter electrode to form superoxide anions ($\cdot O_2^-$). Following a series of reactions with H^+, the activated $\cdot O_2^-$ further produced hydroxyl radicals (·OH), which were responsible for the degradation of organic pollutants [38,39]. On the other hand, Au-NPs are generally stable enough that the plasmon-induced charge separation does not cause their oxidative dissolution [40]. Thus, there may be some species, including intermediates of degraded MO molecules in the present system, that serve as the donors for providing electrons to Au-NPs in photo-excited state. Choosing a suitable donor for the Au/TiO_2-NTs was a feasible way to improving the photoelectrochemical performance. The simplified mechanism of PEC process indicated in Fig. 8 did not show the shift of the Fermi level for the gold-TiO_2 system before and after visible-light irradiation. Whereas many papers discuss the equilibration of Fermi level under UV light illumination [41–43], a limited number of papers discuss the PEC process in detail to date.

To find the evidence for the mechanism of the PEC degradation of aqueous MO in the presence of as-prepared Au/TiO_2-NTs, we carried out the control experiments by purging with N_2 and adding IPA (1.0 mL) or $Na_2C_2O_4$ into the reaction solution, as shown in Fig. 9a. Upon being bubbled with N_2 constantly, O_2 molecules could be completely expelled from the reaction system, inhibiting the formation of $\cdot O_2^-$ and ·OH. It was found that the degradation efficiency of MO decreased greatly, implying that the PEC activity of Au/TiO_2-NTs for degrading organic pollutants was mainly due to the radicals produced from the reaction between the photo-generated electrons from Au-NPs and dissolved O_2. IPA, which can minimize the formation of ·OH, was also utilized to investigate the effect of ·OH on the PEC activity [44]. The results indicated that the degradation rate of MO decreased to 25% upon introducing IPA. As shown in Fig. 9b, the photocatalytic removal rate of MO could also be recognized to follow mass-transfer-controlled first-order-kinetics approximately as a result of low concentration target pollutants under various reaction conditions. In the presence of N_2 or isopropanol (IPA), the rate constants decreased greatly from 0.1678 to 0.0100 and 0.0557, respectively. It should be noted that just a slight decrease (from 0.1678 to 0.1415) of activity resulted from the introduction of $Na_2C_2O_4$ as holes scavengers. This indicated that the role of the holes on the Au surface was not the key for the photoelectrocatalytic performance of the Au/TiO_2-NTs in degrading organic pollutants. The ·OH radicals were further detected by terephthalic acid photoluminescence probing (TA-PL) technique. From Fig. 9c, one can observe that the intensity of the fluorescence peak at 426 nm increased steadily with irradiation time, implying that ·OH radicals can be continuously generated in the reaction system under visible-light illumination. According to the above discussion, we could conclude that the PEC activity for degrading MO of Au/TiO_2-NTs was mainly attributed to ·OH radicals.

4. Conclusions

In summary, Au-NPs-enhanced TiO_2 nanotube arrays were fabricated using the pulse electrodeposition route. The obtained Au/TiO_2-NTs composite electrode possessed highly-dispersed Au-NPs with controllable size, well crystallized TiO_2 anatase phases, strong interaction between Au and TiO_2-NTs, and excellent absorption ability in the visible-light region. These merits mentioned above allowed both high photocurrent response and excellent photoelectrocatalytic activities for degrading organic pollutants under visible-light irradiation ($\lambda > 420$ nm). The synergy effect between nanotubular structures of TiO_2 and uniformly dispersed Au nanoparticles on TiO_2, as well as a small bias potential and the strong interaction between Au and TiO_2, facilitated the plasmon-induced charge separation and transfer, thereby leading to the high-efficiency visible-light PEC activity of Au/TiO_2-NTs. It was also concluded that MO degradation in PEC process was mainly attributed to ·OH radicals produced in the counter electrode. The proposed route can be extended to the design of other hybrid semiconductor-based nanotube electrodes, such as Ag/TiO_2-NTs, Pt/TiO_2-NTs and Pd/TiO_2-NTs, for photoelectrochemical application.

Acknowledgments

This work was supported by the National Natural Science Foundation of China (21207090, 21477079, 21261140333), Shanghai Government (11SG42, 11ZR1426300, 12PJ1406800, 13YZ054, 14ZR1430900), PCSIRT (IRT1269), and by a scheme administrated by Shanghai Normal University (DXL122, and S30406).

Appendix A. Supplementary data

Supplementary data associated with this article can be found, in the online version, at http://dx.doi.org/10.1016/j.apcatb.2014.09.029.

References

[1] Y. Hou, X.Y. Li, X.J. Zou, X. Quan, G.C. Chen, Environ. Sci. Technol. 43 (2009) 858–863.
[2] G.P. Dai, J.G. Yu, G.H. Liu, Environ. Sci. Technol. 44 (2010) 5098–5103.
[3] Y. Hou, X.Y. Li, Q.D. Zhao, X. Quan, G. Chen, J. Phys. Chem. C 115 (2011) 7339–7346.
[4] M.D. Ye, J.J. Gong, Y.K. Lai, C.J. Lin, Z.Q. Lin, J. Am. Chem. Soc. 134 (2012) 15720–15723.
[5] S.S. Zhang, B.Y. Peng, S.Y. Yang, Y.P. Fang, F. Peng, Int. J. Hydrogen Energ. 38 (2013) 13866–13871.
[6] Y. Hou, X.Y. Li, Q.D. Zhao, G.H. Chen, C.L. Rastor, Environ. Sci. Technol. 46 (2012) 4042–4050.
[7] X.L. Liu, Y.H. Han, G.Y. Li, H.M. Zhang, H.J. Zhao, RSC Adv. 3 (2013) 20824–20828.
[8] G.K. Mor, K. Shankar, M. Paulose, O.K. Varghese, C.A. Grimes, Appl. Phys. Lett. 91 (2007) 152111.
[9] T. Rattanavoravipa, T. Sagawa, S. Yoshikawa, Sol. Energ. Mat. Sol. C 92 (2008) 1445–1449.
[10] Z.W. Seh, S.H. Liu, M. Low, S.Y. Zhang, Z.L. Liu, A. Mlayah, M.Y. Han, Adv. Mater. 24 (2012) 2310–2314.
[11] C.G. Silva, R. Juarez, T. Marino, R. Molinari, H. Garcia, J. Am. Chem. Soc. 133 (2011) 595–602.
[12] A. Corma, P. Serna, H. Garcia, J. Am. Chem. Soc. 129 (2007) 6358–6359.
[13] I. Paramasivalm, J.M. Macak, P. Schmuki, Electrochem. Commun. 10 (2008) 71–75.
[14] D.F. Zhang, Russ. J. Phys. Chem. A 86 (2012) 498–503.
[15] M. Maicu, M.C. Hidalgo, G. Colon, J.A. Navio, J. Photochem. Photobiol. A-Chem. 217 (2011) 275–283.
[16] S. Oros-Ruiz, R. Zanella, R. Lopez, A. Hernandez-Gordillo, R. Gomez, J. Hazard. Mater. 263 (2013) 2–10.
[17] Y.K. Lai, H.F. Zhuang, K.P. Xie, D.G. Gong, Y.X. Tang, L. Sun, C.J. Lin, Z. Chen, New J. Chem. 34 (2010) 1335–1340.
[18] M.S. Chandrasekar, M. Pushpavanam, Electrochim. Acta 53 (2008) 3313–3322.
[19] X.L. Li, J.Y. Yao, F.L. Liu, H.C. He, M. Zhou, N. Mao, P. Xiao, Y.H. Zhang, Sensor. Actuat. B: Chem. 181 (2013) 501–508.
[20] Y.H. Zhang, Y.N. Yang, P. Xiao, X.N. Zhang, L. Lu, L. Li, Mater. Lett. 63 (2009) 2429–2431.
[21] L. Assaud, V. Heresanu, M. Hanbucken, L. Santinacci, Comptes Rendus Chimie 16 (2013) 89–95.
[22] L.X. Yang, S.L. Luo, F. Su, Y. Xiao, Y.F. Chen, Q.Y. Cai, J. Phys. Chem. C 114 (2010) 7694–7699.
[23] M.S. Chandrasekar, M. Shanmugasigamani, Pushpavanam, Mater. Chem. Phys. 115 (2009) 603–611.
[24] J.C. Fuggle, N. Martensson, J. Electron. Spectrosc. Relat. Phenom. 21 (1980) 275–281.
[25] N. Kruse, S. Chenakin, Appl. Catal. A: Gen. 391 (2011) 367–376.

[26] Z.H. Zhang, L.B. Zhang, M.N. Hedhili, H.N. Zhang, P. Wang, Nano Lett. 13 (2013) 14–20.
[27] H.M. Zhu, B.F. Yang, J. Xu, Z.P. Fu, M.W. Wen, T. Guo, S.Q. Fu, J. Zuo, S.Y. Zhang, Appl. Catal. B: Environ. 90 (2009) 463–469.
[28] K.L. Kelly, E. Coronado, L.L. Zhao, G.C. Schatz, J. Phys. Chem. B 107 (2002) 668–677.
[29] M. Murdoch, G.I.N. Waterhouse, M.A. Nadeem, J.B. Metson, M.A. Keane, R.F. Howe, J. Llorca, H. Idriss, Nat. Chem. 3 (2011) 489–492.
[30] W. Haiss, N.T.K. Thanh, J. Aveyard, D.G. Fernig, Anal. Chem. 79 (2007) 4215–4221.
[31] L.M. Liz-Marzán, Langmuir 22 (2005) 32–41.
[32] T. Kawawaki, Y. Takahashi, T. Tatsuma, J. Phys. Chem. C 117 (2013) 5901–5907.
[33] G.V. Hartland, Chem. Rev. 111 (2011) 3858–3887.
[34] S.K. Ghosh, T. Pal, Chem. Rev. 107 (2007) 4797–4862.
[35] Z.F. Bian, J. Zhu, F.L. Cao, Y.F. Lu, H.X. Li, Chem. Commun. 378 (2009) 9–3791.
[36] G.S. Li, L. Wu, F. Li, P.P. Xu, D.Q. Zhang, H.X. Li, Nanoscale 5 (2013) 2118–2125.
[37] Y. Tian, T. Tatsuma, J. Am. Chem. Soc. 127 (2005) 7632–7637.
[38] K.P. Xie, L. Sun, C.L. Wang, Y.K. Lai, M.Y. Wang, H.B. Chen, C. Lin, J. Electrochim. Acta 55 (2010) 7211–7218.
[39] G.S. Li, B. Jiang, S.N. Xiao, Z.C. Lian, D.Q. Zhang, J.C. Yu, H.X. Li, Environ. Sci. 16 (2014) 1975–1980.
[40] Y. Konishi, I. Tanabe, T. Tatsuma, Dalton Trans. 42 (2013) 15937–15940.
[41] A. Wood, M. Giersig, P. Mulvaney, J. Phys. Chem. B 105 (2001) 8810–8815.
[42] M. Jakob, H. Levanon, P.V. Kamat, Nano Lett. 3 (2003) 353–358.
[43] V. Subramanian, E.E. Wolf, P.V. Kamat, J. Am. Chem. Soc 126 (2004) 4943–4950.
[44] B. Jiang, P. Zhang, Y. Zhang, L. Wu, H.X. Li, D.Q. Zhang, G.S. Li, Nanoscale 4 (2012) 455–460.